J. Fluid Mech. (1983), *vol.* 132, *pp.* 271–281
Printed in Great Britain

A note on the stability of low-Prandtl-number Hadley circulations

By JOHN HART

Department of Astrogeophysics, University of Colorado, Boulder, Colorado 80309

(Received 25 January 1982 and in revised form 8 December 1982)

This paper discusses the stability of the flow of a low-Prandtl-number liquid contained in a shallow slot with differentially heated vertical endwalls. The effect of thermally insulating boundaries at the top and bottom of the container on wavelength selection is emphasized. Stability calculations indicate that, for Prandtl number Pr in the range $0.015 < Pr < 0.27$, the first perturbations to grow are overstable (oscillatory) longitudinal rolls with axes perpendicular to the endwalls, and with very large cross-stream wavelengths of about 9 to 15 layer depths. Previous studies using thermally conducting boundaries predict critical wavelengths of about three layer depths. The new results are in substantial agreement with an experiment using a differentially heated layer of mercury with aspect ratio (depth/length) 0.047 in both horizontal directions. The implications of the long-wavelength instability for the interpretation of thermal oscillations observed in other smaller-aspect-ratio configurations is discussed.

1. Introduction

We consider the flow in a rectangular cavity as shown in figure 1. Motion is driven by heating a fluid differentially at the two endwalls. At small ΔT a simple unicellular flow is established where motion is up the hot wall, across the top, down the cold wall and returning across the bottom. Such simple thermally direct single-cell flows have come to be known as Hadley circulations. Experimental studies of such flows using low-Prandtl-number fluids like molten gallium (Hurle, Jakeman & Johnson 1974) indicate that, as ΔT is increased beyond a critical value ΔT_c, thermal oscillations appear spontaneously. Hart (1972, hereinafter H72), showed that model Hadley cells could be unstable to oscillating rolls oriented perpendicular to the end walls. Subsequently Gill (1974) proposed this instability as the cause of the observed oscillation, and constructed an approximate theory that roughly agreed with the experiments of Hurle *et al.* and of Skafel (1972, reported in Gill's paper). However, previous theories have not dealt correctly with the experimental boundary conditions at $z^* = \pm\frac{1}{2}D$. For example, H72 studied rigid conductors, Gill (1974) in essence studied free conductors, while the experiments have either rigid insulators or a rigid insulator and a free insulator. The purpose of this paper is to assess the importance of the vertical boundary conditions on the stability properties of the Hadley flow. Substantial effects are found, and these have led to a new experiment that satisfies the fundamental constraints on the theory better.

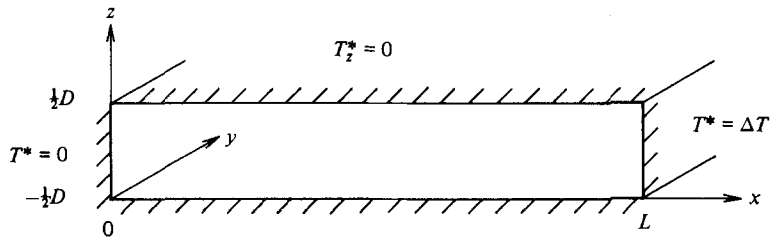

FIGURE 1. Basic geometry and thermal boundary conditions.

2. The basic flow

Consider the steady flow in the cavity of figure 1. In general the Navier–Stokes equations can be normalized using the scales D^2/ν, D, $g\alpha\Delta TD^3/L\nu$, $\Delta TD/L$ for time, length, velocity and temperature respectively. Here g is the gravitational acceleration, ν the kinematic viscosity, α the coefficient of thermal expansion, ΔT the endwall temperature difference, D the fluid depth and L the length of the container. The non-dimensional Boussinesq equations are

$$\frac{\partial \boldsymbol{v}}{\partial t} + Gr\,\boldsymbol{v}\cdot\nabla\boldsymbol{v} = -\nabla p + T\hat{\boldsymbol{z}} + \nabla^2\boldsymbol{v}, \tag{1}$$

$$\frac{\partial T}{\partial t} + Gr\,\boldsymbol{v}\cdot\nabla T = \frac{\nabla^2 T}{Pr}. \tag{2}$$

The control parameters are the Grashof number

$$Gr = \frac{g\alpha\Delta TD^4}{\nu^2 L}$$

and the Prandtl number

$$Pr = \frac{\nu}{\kappa}.$$

As discussed in H72 and Cormack, Leal & Imberger (1974), if the slot aspect ratio $\epsilon = D/L$ is sufficiently small, then a simple exact parallel-flow solution will exist away from thin turning regions near the endwalls. The parallel flow arises in response to a lateral temperature gradient. Advection of heat by this end-to-end counterflow is then balanced by vertical diffusion. The form of the solutions depend on the top and bottom boundary conditions at $z = \pm\frac{1}{2}$. For rigid insulators at both surfaces:

$$V_0 = W_0 = 0,$$

$$U_0 = a(\tfrac{1}{6}z^3 - \tfrac{1}{24}z), \tag{3}$$

$$T_0 = ax + \tfrac{1}{6}Gr\,Pr\,a(\tfrac{1}{20}z^5 - \tfrac{1}{24}z^3 + 0.0015625). \tag{4}$$

If the upper surface is a stress-free insulator, then with $z' = z + \frac{1}{2}$,

$$U_0 = a(\tfrac{1}{6}z'^3 - \tfrac{5}{16}z'^2 + \tfrac{1}{8}z'). \tag{5}$$

$$T_0 = ax + Gr\,Pr\,a(\tfrac{1}{120}z'^5 - \tfrac{5}{192}z'^4 + \tfrac{1}{16}z'^2 + b), \tag{6}$$

where the constant b is chosen so that there is no net advective heat flux at any x. Since only gradients of T_0 appear in the stability problem, its value is largely irrelevant here.

The constant a in these solutions is formally obtained by matching these parallel flows to the turning flow in the two end regions. This has been done by Cormack *et*

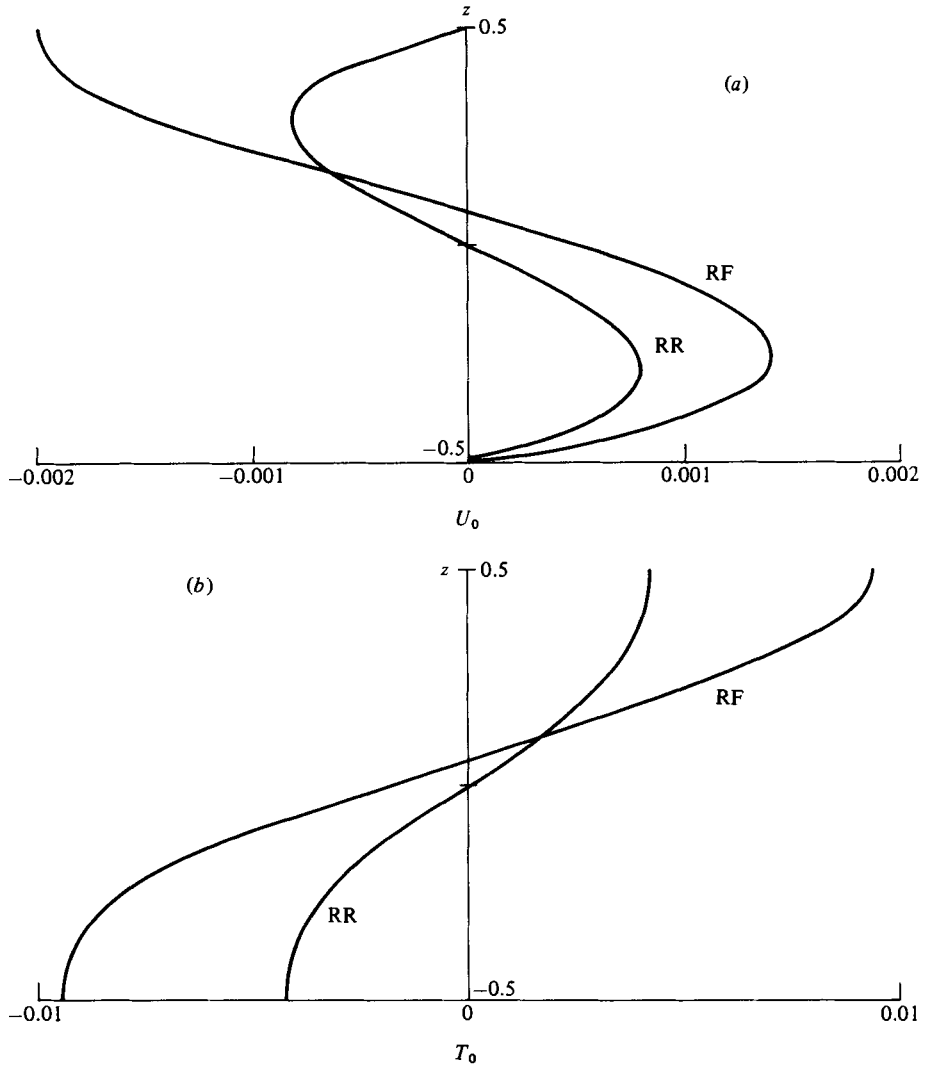

FIGURE 2. (*a*) Basic velocity profiles. RR = rigid top and bottom. RF = rigid bottom, stress-free top. (*b*) Basic thermal fields, z-dependent parts.

al. (1974) for Pr and $Gr = O(1)$, and by Hart (1983) for Pr small and $Gr\,\epsilon^2 = O(1)$, in the small-ϵ limit. To leading order in ϵ, Hart (1983) finds a relationship, nearly identical with that derived by Cormack *et al.*,

$$a = 1 - 3.44 \times 10^{-6} F(Gr, Pr)\, Gr^2\, Pr^2\, \epsilon + O(\epsilon^2), \tag{7}$$

where $F(Gr, Pr)$ is a function that varies by about 20% from 1 over the range of Gr and Pr of interest for the stability considerations. This gives one limit to the validity of the interior parallel-flow solution. We assume the apparatus is shallow enough that $a = 1$ yields an accurate approximation to the actual interior Hadley circulation.

The basic-flow profiles are shown in figure 2. In both physical cases the vertically varying parts of T_0 are statically stable everywhere. This is contrasted with the rigid conducting solutions of H72 where thin statically unstable regions exist near $z = \pm\frac{1}{2}$. In the present case, no classical convective modes of instability are expected. We proceed to consider the stability of the above basic states. In what follows we shall

refer to the case with two rigid and insulating boundaries as 'rigid–rigid' (RR), and the case with one rigid insulator below an upper stress-free insulator as 'rigid–free' (RF).

3. The stability problem

The governing equations are linearized about either (3) and (4) or (5) and (6). We consider two types of disturbance. Transverse modes have axes perpendicular to the basic flow and have form

$$w, T = \{w(z), T(z)\}\, e^{\omega t}\, e^{ikx}.$$

For small Pr, these turn out to be the classical shear waves, studied by Birikh (1966), modified here by the basic thermal field and associated perturbation advections. The perturbation equations for this mode are

$$\omega(d^2-k^2)\, w + ik\, Gr\, [U_0(d^2-k^2)\, w - w d^2 U_0] + k^2 T = (d^2-k^2)^2\, w, \tag{8}$$

$$Pr\, \omega T + ik\, Ra\, U_0 T + Ra\, w T_0 z + \frac{iRa\, \mathrm{d}w}{k} = (\mathrm{d}^2-k^2)\, T,$$

where $Ra = Gr\, Pr$, and $\mathrm{d} = \mathrm{d}/\mathrm{d}z$.

Longitudinal modes have axes parallel to the basic flow. They depend only on z and y, not x, so that

$$u, w, T = \{u(z), w(z), T(z)\}\, e^{\omega t}\, e^{iky}.$$

The perturbation equations for the longitudinal modes are

$$\omega(\mathrm{d}^2-k^2)\, w + k^2 T = (\mathrm{d}^2-k^2)^2\, w, \tag{10}$$

$$\omega u + Gr\, w U_{0z} = (\mathrm{d}^2-k^2)\, u, \tag{11}$$

$$Pr\, w T + Ra\, u + Ra\, w T_{0z} = (\mathrm{d}^2-k^2)\, T. \tag{12}$$

The above equations and perturbation energetics have been discussed in detail in H72. It is useful here to examine the mechanism for the longitudinal instability since it is not as well known as that for the transverse shear mode. Consider a case where U_{0z} is approximately constant (for example the region near $z = 0$ in figure 2a). Also consider Gr and Pr large enough so that dissipative effects are small. Then, as $Pr \to 0$ ($Gr\, Pr$ large), the T_{0z} term will not enter, and (10)–(12) become simply

$$\omega(\mathrm{d}^2-k^2)\, w + k^2 T = 0,$$

$$\omega u + Gr\, w U_{0z} = 0,$$

$$\omega T + Gr\, u = 0.$$

With an assumed $w \propto \cos \pi z$, the eigenvalue ω is given by

$$\omega^3 = Gr^2 k^2 U_{0z} (\pi^2 + k^2)^{-1}. \tag{13}$$

Equation (13) predicts a monotonic instability if $U_{0z} > 0$; Hart (1971) gives a theoretical and experimental study of this mode in a somewhat different context. However, if $U_{0z} < 0$, an overstable mode should appear. H72 and Gill (1974) give physical interpretations. Of importance here is the tendency for the frequency of the oscillation to increase with both Gr and k. The basic Hadley circulation has shear of both signs, so both the monotonic mode and oscillatory mode are possible. Further progress with the full problem including proper boundary conditions requires numerical solution of (8)–(12).

The stability problem is solved by the Galerkin method, which reduces the ODEs

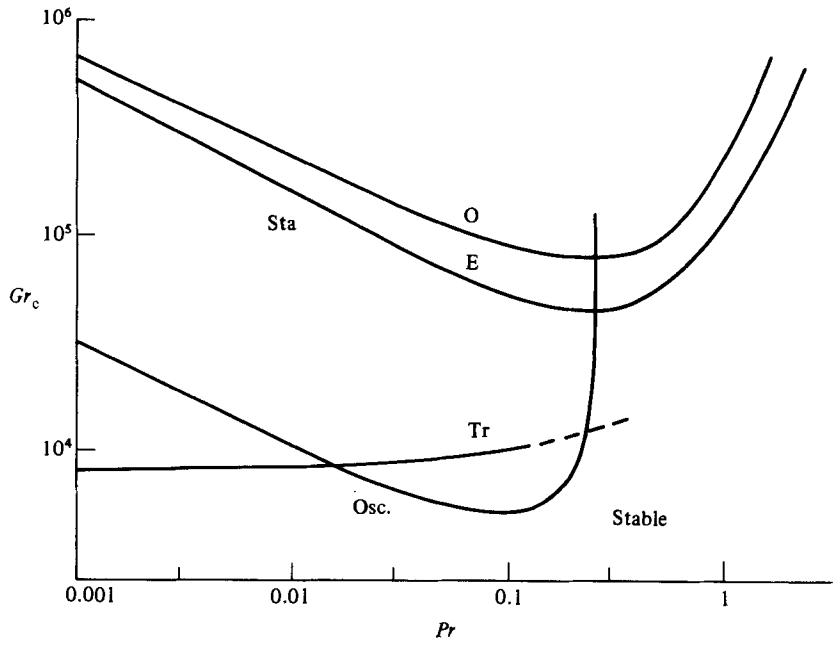

FIGURE 3. Neutral curves for RR boundaries. Osc = oscillatory even longitudinal modes. Sta E, O = stationary even and odd longitudinal modes. Tr = transverse stationary modes.

to a real matrix eigenvalue problem that is solved by the QR-algorithm. The trial functions for the various boundary conditions are given in the appendix. For the longitudinal rigid–rigid problem there are non-combining even and odd modes (E and O). For the other problems the even and odd modes are coupled.

Figure 3 shows the neutral curves for the rigid–rigid case. For moderately small Pr the overstable mode is the first to become unstable as Gr is increased. It cuts off at $Pr = 0.27$. If Pr is made too large, the stabilizing effect of T_{0z}, proportional to Ra^2, overpowers the lateral gradient buoyancy generation, proportional to Ra, no matter how big Gr is made. As Pr approaches zero, Gr_c increases because thermal diffusion damps the instability. The oscillatory mode is dominated by the lowest even eigenfunction. That is, the thermal perturbation is almost independent of z. This is allowed of course, because the boundaries are insulators. When Pr is small the perturbation tries to minimize the relatively large thermal diffusion by having such a z-independent structure. Thus $(\mathrm{d}^2 - k^2)T$ becomes approximately $-k^2T$. Thus to further minimize the dominant thermal dissipation the *most-unstable oscillatory modes have very small* k. This is shown in figure 4. For mercury, $Pr = 0.026$, the oscillatory longitudinal mode with $k = 0.7$ is the most-unstable disturbance.

In addition to the oscillatory mode, stationary longitudinal modes at much higher Gr and k are possible, being possibly the most unstable at higher Pr. The transverse-wave calculation did not converge very well for Pr larger than about 0.1, but it is likely that these modes can also exist at $Pr \approx 1$. The monotonic longitudinal modes have small vertical scales, and lie in the space near the walls at $z = \pm\frac{1}{2}$ where $U_{0z} > 0$. As such they can have larger k (and hence larger buoyancy generation k^2T) before the diffusion operator $(\mathrm{d}^2 - k^2)$ becomes dominated by k^2.

A similar situation exists for the case with rigid–free boundaries. Figure 5 shows the neutral curves for $Pr = 0.001$–1. The most-unstable mode is longitudinal-oscillatory, and again k is very small (figure 4). No other longitudinal modes of

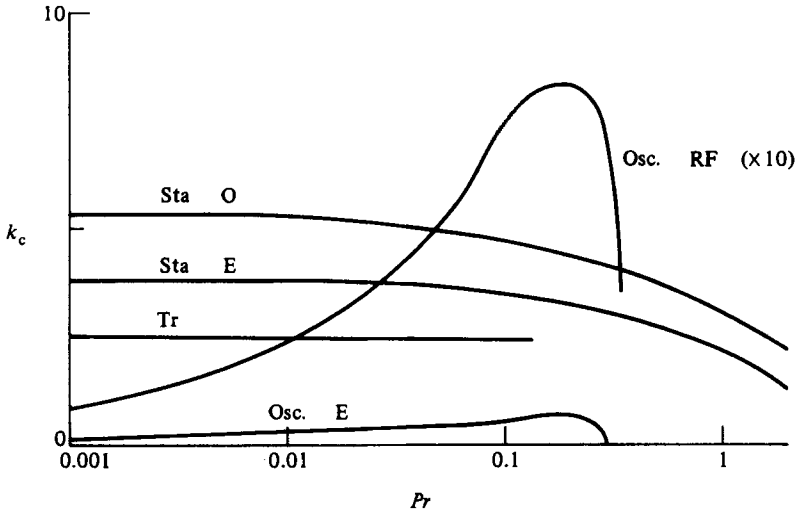

FIGURE 4. Critical wavenumbers for moves in figures 3 and 5. All are for RR unless noted.

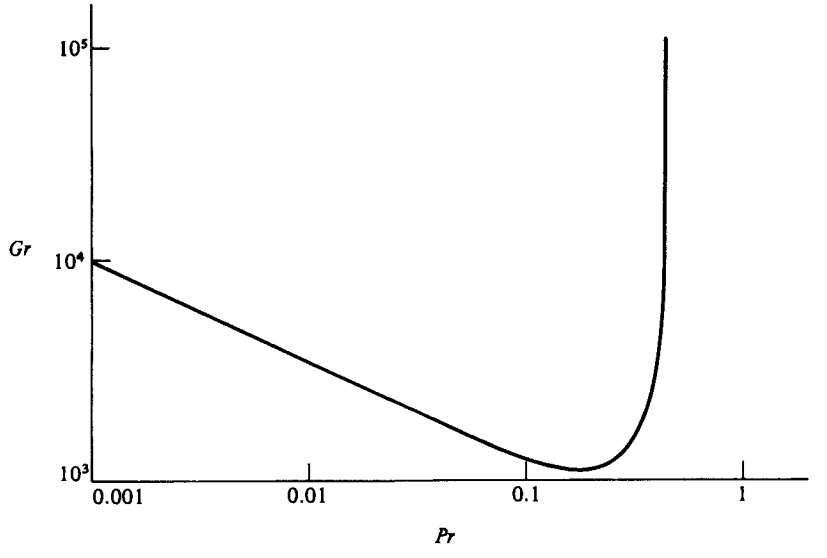

FIGURE 5. Neutral curve for longitudinal modes, case RF.

instability were found over the range of Gr and Pr shown in the figure. Some transverse disturbances may exist, but they were not determined owing to computational limitations explained in the appendix. For the oscillatory RF mode the critical Grashof number is lower than in the RR case because the relaxed boundary condition at $z = \frac{1}{2}$ allows a larger basic shear near $z = 0$ and a larger perturbation velocity u.

Figure 6 shows that the predicted critical frequencies for the longitudinal oscillatory modes are relatively constant except near the Pr cutoffs. On the other hand, at fixed Pr and increasing supercriticality $(Gr - Gr_c)/Gr$, both the most rapidly growing wavenumber k and frequency ω_i increase. This is shown in figure 7 for the RR case. A similar monotonic increase of the k that maximized ω_r, and ω_i, with Gr was found for the RF oscillatory mode. These results reflect the simple prediction of (13).

In conclusion, the theory predicts a long-wavelength, longitudinal, oscillatory

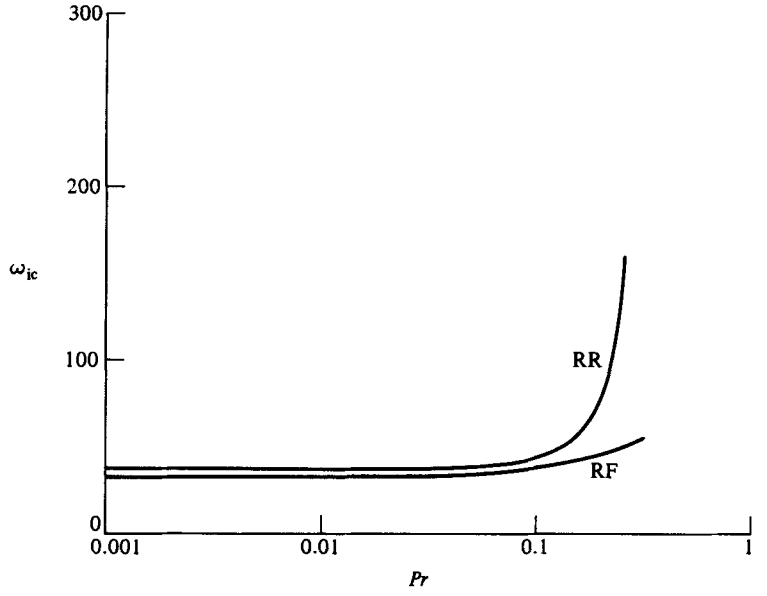

FIGURE 6. Critical frequency for the longitudinal oscillatory modes.

instability for small-aspect-ratio Hadley circulations with a Prandtl number between about 0.015 and 0.27. It should be observable in liquid metals, but not in higher-Pr fluids like air or water. In these substances the dominant mode of instability will be either stationary longitudinal rolls, or more probably, transverse shear waves. It should be noted, however, that (7) suggests that it may be difficult to realize the basic state used here in the higher-Pr fluids. In comparison with the rigid-conducting case (H72), the roll wavelength here is about 3 times bigger, the critical Gr about 3 times smaller, and longitudinal oscillations are preferred over transverse stationary modes for the range of Prandtl number cited above.

4. Comparison with experiments

The major difference between the present results and previous theoretical results of Gill (1974), H72, and others, is that the low-Prandtl-number oscillatory instability with insulating upper and lower boundaries typical of all past experimental studies should occur at large wavelengths. Since most previous experiments were performed at relatively large aspect ratios, so that only about one roll (one half of a critical wavelength) could fit across the apparatus, it was decided to conduct a new experiment with as small an aspect ratio in both directions as possible. Our major comparison is with an experiment using mercury in a cell with $D = 1.2$ cm, $L = 21$ cm, and $Ly = 21$ cm, where Ly denotes the dimension in the cross-stream or cross-roll direction. Thus the aspect ratio is $\epsilon = 0.047$, and the cell can hold about 5 of the fastest-growing rolls as predicted by the theory. Attempts to attain still smaller ϵ would lead to prohibitively long equilibration times L^2/k and unwanted thermal boundary flux effects. The cost of mercury was another limiting factor.

The cell was constructed out of 1.2 cm Perspex, with machined stainless-steel water jackets at the two ends. The water baths had long-term stability of 0.02 °C compared with an onset temperature difference of about 1 °C. The apparatus was levelled and isolated by surrounding the cell with foam insulation. The experiment was carried

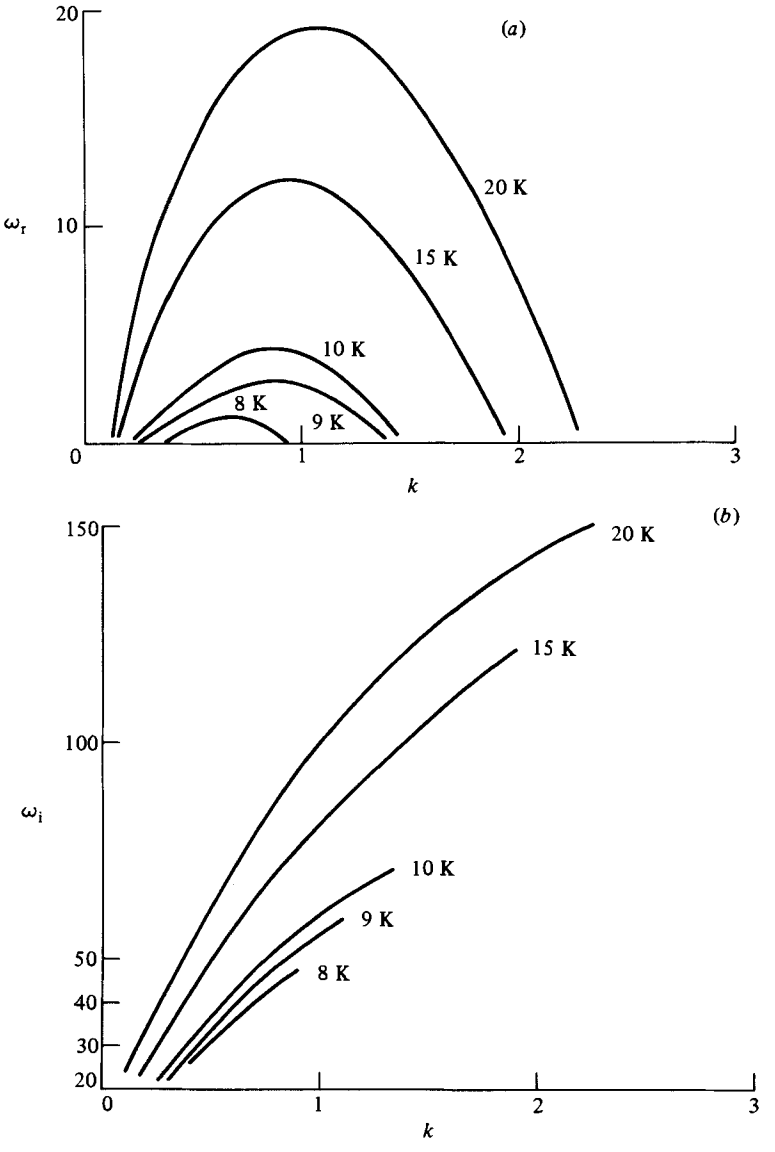

FIGURE 7. Supercritical ω-values for the RR case; $Pr = 0.026$. Curves for values of Gr shown (K $\equiv \times 1000$).

out by measuring the first appearance of oscillations with a 0.1 mm glass-enclosed thermistor probe inserted through a small hole in the upper lid. By using a phase-locked amplifier, sensitivity of 0.001 °C was easily obtained. The imposed temperature difference was increased by 5%/24 hr until oscillations were observed.

The thermistor measurements accurately determine the critical value of Gr for the first appearance of the oscillatory instability, as well as the critical frequency. The wavelength was measured by replacing the upper lid of the cell with a piece of Perspex that had a liquid-crystal thermometer sheet (Edmund Scientific Co., Gt Barrington, N.J.) in contact with the upper mercury surface. It serves as a rigid insulating boundary and reflects blue light when in contact with a liquid 5 °C above its ambient operating point (here 25 °C) and red when the liquid is at the ambient point. Hence

Author		ϵ	L_y/D	$Gr_{c\,exp}$	$\frac{1}{2}K_{min\,exp}$	$\omega_{i\,exp}$	$\omega_{ith}(Gr_c, \frac{1}{2}k_{min})$ RF	RR
Skafel	*A*	0.15	6.4	1.6×10^4	0.49	56	53	57
(from Gill)	*B*	0.2	4.8	1.4×10^4	0.65	62	64	73
$Pr = 0.026$								
Hurl *et al.*	*C*	0.21	2.0	2.5×10^4	1.58	113	180	152
$Pr = 0.02$	*D*	0.29	1.5	7.0×10^4	2.09	247	570	390

TABLE 1. Comparisons with previous experiments

photographs of the sheet from above yield colour contours of the total temperature field. For optimal performance it is necessary to photograph at supercritical conditions with a 5 °C drop across the cell, but the wavelength of weak oscillations can also be measured. Figure 8 (plate 1) shows two photographs at supercritical conditions where the perturbations across the tank are clearly visible. There are roughly 5 rolls that oscillate periodically and disturb the normal lateral thermal gradient associated with the basic state.

For this experiment with $Pr = 0.026$, the theory predicts the following critical quantities: $Gr = 7.1\times10^3$, $k_c = 0.71$, $\omega_i = 36.5$. The experimental values are $Gr = 9.3\times10^3$, $k_c = 0.8\pm0.1$, $\omega_i = 54\pm4$. The agreement is reasonable, considering that the aspect ratio is still rather large, since at such low predicted and observed wavenumbers it is hard to get a purely longitudinal disturbance. Using figure 7 we can evaluate the predicted frequency in terms of the observed Gr and k to get a new theoretical value of $\omega_i = 49$ that is in better agreement with experiment. Further predictions of figure 7 are verified by data at higher $Gr = 1.8\times10^4$ where the experimental frequency is $\omega_i = 92\pm5$ compared with a theoretical value of $\omega_i = 83$. Thus the experiment confirms the major predictions of the theory; that the dominant instability is a longitudinal oscillatory one of low wavenumber whose energy source is the basic lateral temperature gradient of the Hadley cell.

It is clear that with a critical wavelength of $9D$–$16D$ depending on Pr and the upper boundary condition, moderate-aspect-ratio experiments will show unstable disturbances strongly influenced by sidewalls. Table 1 shows an attempt to compare the theory with typical observations of previous investigators. The value $\frac{1}{2}k_{min}$ gives the smallest k that would allow one roll to fit across the experimental apparatus. Except for case *A* there is a strong mismatch between box size and the preferred k. From the theory $Gr_c = 7.1\times10^3$ for mercury and 6.9×10^3 for gallium. It is obvious that there are strong geometric effects present experimentally that are not accounted for in the theory, In the gallium experiments the fact that the measured critical values of Gr are so much higher than the predicted value probably also reflects a severely modified basic thermal field with either a becoming very small, or some sort of a non-parallel basic flow being present. One should also note the very low theoretical growth rates near critical. For mercury and a depth of 1 cm at 14 % supercriticality, the e-folding time is about 3000 s. It may then be difficult to observe the unstable rolls extremely close to the critical Gr. The predicted frequencies at the observed values of Gr and $k = \frac{1}{2}k_{min}$ are within a factor of two of the observations, suggesting the longitudinal roll instability is present though strongly modified by the finite aspect ratio.

This research was sponsored by the National Science Foundation, Grant ATM 81-11718.

Appendix. Trial functions and truncation levels

A.1. *Longitudinal modes, rigid–rigid insulators*

These have $$u(\pm\tfrac{1}{2}) = w(\pm\tfrac{1}{2}) = w_z(\pm\tfrac{1}{2}) = T_z(\pm\tfrac{1}{2}) = 0.$$

We take $$w = \sum_{i=1}^{N} a_i E_i(\lambda_i z) + b_i O_i(\mu_i z),$$

where $$E_i = \frac{\cosh\lambda_i z}{\cosh\tfrac{1}{2}\lambda_i} - \frac{\cos\lambda_i z}{\cos\tfrac{1}{2}\lambda_i},$$

$$O_i = \frac{\sinh\lambda_i z}{\sinh\tfrac{1}{2}\lambda_i} - \frac{\sin\lambda_i z}{\sin\tfrac{1}{2}\lambda_i}$$

with $$\tanh\tfrac{1}{2}\lambda_i + \tan\tfrac{1}{2}\lambda_i = 0,$$

$$\coth\tfrac{1}{2}\mu_i + \cot\tfrac{1}{2}\mu_i = 0.$$

Also $$u = \sum_{i=1}^{N} c_i \cos(2i-1)\pi z + \mathrm{d}_i \sin(2i\pi z)$$

$$T = \sum_{i=1}^{N} e_i \cos 2(i-1)\pi z + f_i \sin(2i-1)\pi z.$$

This expansion yields a $3N \times 3N$ matrix eigenvalue problem. Accurate eigenvalues are obtained with $N = 8$. Earlier work (H72) failed to include the z-independent thermal mode, and therefore was in error for these boundary conditions.

A.2. *Longitudinal modes, rigid–free insulators*

For convenience we transform to the region $z = (0, 1)$. The boundary conditions are

$$u(0) = u_z(1) = w(0) = w_z(1) = T_z(1) = w(1) = T_z(0) = w_{zz}(1) = 0.$$

We take $$w = \sum_{i=1}^{N} a_i \left\{ \frac{\mathrm{e}^{-\lambda_i z} - \mathrm{e}^{\lambda_i(z-2)}}{1-\mathrm{e}^{-2\lambda_i}} + \frac{\sin\lambda_i z}{\tan\lambda_i} - \cos\lambda_i z \right\},$$

with $$\tanh\lambda_i - \tan\lambda_i = 0.$$

Also $$u = \sum_{i=1}^{N} b_i \sin\tfrac{1}{2}(2i-1)\pi z, \quad T = \sum_{i=1}^{N} c_i \cos(i-1)\pi z.$$

Convergence tests indicate that $N = 8$ gives ω to within 0.1 % of $N = 16$.

A.3. *Transverse modes*

These were computed only for the double-rigid-insulator case. The rigid–free case yields a complex matrix since the basic state is non-symmetric. These modes are expensive to compute (double precision is necessary for $Pr \gtrsim 0.1$), so we limit our study to one case, these modes being of less interest. The eigenfunctions were the same as in §A.1 above. They are unfortunately not very efficient, and $N = 14$ was necessary for $Pr = 0$. Beyond $Pr = 0.1$ our scheme did not converge very well, and as this is outside our region of interest we have not pursued calculations beyond this point.

The calculations were performed on a VAX 11/750 with $6\frac{1}{2}$ digit arithmetic. The earlier study (H72) used a CDC6600 with 12-digit precision.

REFERENCES

BIRIKH, R. V. 1966 On small perturbations of a plane parallel flow with a cubic velocity profile. *J. Appl. Maths Mech.* **30**, 432.

CORMACK, D. E., LEAL, L. G. & IMBERGER, J. 1974 Natural convection in a shallow cavity with differentially heated end walls. Part 1. Asymptotic theory. *J. Fluid Mech.* **65**, 209.

GILL, A. E. 1974 A theory of thermal oscillations in liquid metals. *J. Fluid Mech.* **64**, 577.

HART, J. E. 1971 Stability of the flow in a differentially heated inclined box. *J. Fluid Mech.* **47**, 547.

HART, J. E. 1972 Stability of thin non-rotating Hadley circulations. *J. Atmos. Sci.* **29**, 687.

HART, J. E. 1983 Low Prandtl number convection driven between differentially heated end walls. *Intl J. Heat Mass Transfer* (to appear).

HURLE, D. T. J., JACKMAN, E. & JOHNSON, C. P. 1974 Convective temperature oscillations in molten gallium. *J. Fluid Mech.* **64**, 565.